Optical Fiber Technology 58 (2020) 102267

Contents lists available at ScienceDirect

Optical Fiber Technology

journal homepage: www.elsevier.com/locate/yofte

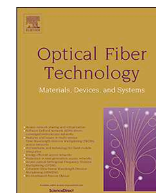

Nanoscale curved dielectric film characterization beyond diffraction limits using spatially structured illumination

Enes Ataç[a,*], Mehmet Salih Dinleyici[a]

[a] Department of Electrical and Electronics Engineering, Izmir Institute of Technology, Izmir, Turkey

ARTICLE INFO

Keywords:
Diffraction limit
Structured illumination
Sub-wavelength dielectric films
Phase diffraction

ABSTRACT

Optical fiber based sensor systems often utilize thin dielectric films coated on non-planar surfaces are needed to be inspected for quality assurance. However, non-destructive optical characterization of these films is not a simple method especially on curved large surfaces. In this study, we propose a real time procedure to estimate the optical properties of sub-wavelength transparent dielectric films coated on optical fibers. The paper includes developing a mathematical model and its experimental verification. The near field phase diffraction method is combined with the structured light illumination that is spatial modes of optical fibers to estimate the thickness of the phase object beyond the classical diffraction limits. Numerical simulations and experimental results show that the film thickness can safely be characterized up to one tenth of wavelength of interest via selective spatial field distribution determined according to the morphology of the thin film. The outcomes have good agreements with destructive Scanning Electron Microscope (SEM) measurements.

1. Introduction

Optical characterization of transparent dielectric optical thin films is a critical issue due to their importance in optical fiber sensor technologies [1,2]. In general, typical fiber optic sensors are based on periodic refractive index modulation inscribed in optical fiber known as Fiber Bragg Grating (FBG) [3–5]. They have wide range applications such as sensing element (temperature, pressure, strain etc.), interrogator, and transducer [6–11]. To get further response from ambient accordingly increase the precision, FBGs are conjuncted with thin films [12–15]. Therefore, well defined optical parameters of thin films becomes an essential task to assure sensing capabilities. However, the thickness of such films are usually fraction of the wavelength. The methods in the literature and commercially available systems generally depend on interferometric techniques [16,17] and ellipsometric techniques [18,19]. Since they are generally scanning and pointwise methods, the characterization becomes tedious and time consuming process especially on curved surfaces. In addition to their complexity, they are mostly expensive.

Optical resolution is a key parameter to resolve spatial features of an object. The resolution of an optical system is limited by the diffraction of light and can be characterized by total point spread function (PSF) of the overall system [20]. In classical diffraction theory, the diffraction limits can be circumvented by reducing the wavelength or increasing numerical aperture, thereby making PSF narrower. However, it can also be improved by a technique PSF engineering rather than conventional methods [21]. The technique uses an idea that the total PSF is product of the excitation and detection PSFs which offer an insight into that the resolution can be increased through selective excitation. This is also fundamental concept of the confocal microscopy and it can be adaptable to the optical thin film characterization methods. Since the PSF of a system is a function of spatial field distribution and coordinates of light source, the film thickness can be estimated better than half of source wavelength via choosing proper illumination according to the morphology of thin film. It is a promising efficient method for curved surfaces having an uneasy geometric shape.

Phase of the diffracted field from a phase object is more sensitive to refractive index variation than amplitude and carries supplementary informations about the system [22]. Since the incident wavefront is modified by the curved geometry through the optical path length of the thin film, it makes a phase contribution to the resultant diffraction pattern. This idea has been exploited in a previous work for the thickness estimation of the transparent dielectric optical thin film about half of the wavelength on the curved substrate by using plane wave illumination [23]. However, the whole information about an optical system can be obtained via increasing the bandwidth of spatial frequencies. Therefore, the near field phase diffraction method becomes fundamental requirement for sub-wavelength optical characterizations

* Corresponding author.
E-mail addresses: enesatac@iyte.edu.tr (E. Ataç), salihdinleyici@iyte.edu.tr (M.S. Dinleyici).

https://doi.org/10.1016/j.yofte.2020.102267
Received 22 April 2020; Received in revised form 12 May 2020; Accepted 14 May 2020
Available online 15 July 2020
1068-5200/ © 2020 Elsevier Inc. All rights reserved.

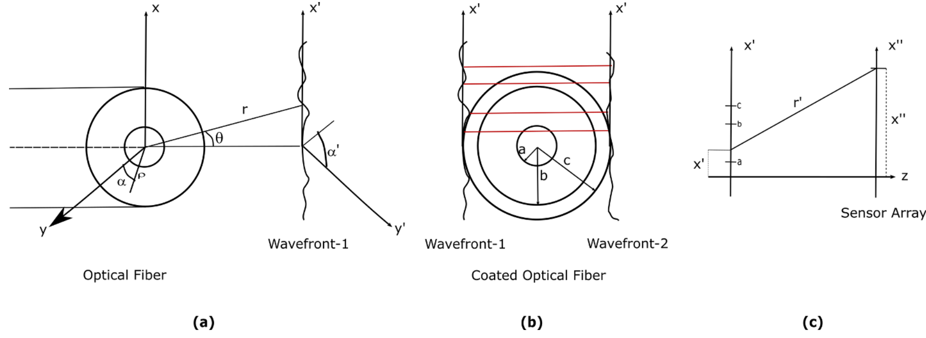

Fig. 1. (a) Far field radiation geometry of structured light from optical fiber end. (b) Paraxial complex ray tracing. (c) Near field Huygens Fresnel diffraction geometry.

otherwise the exponential decaying field components (evanescent waves) are lost and some of spatial frequencies filtered out from the near field to the far field [24].

In this study, we aimed to propose a practical procedure for the estimation of the sub-wavelength thickness transparent dielectric films coated on the optical fiber around one tenth of source wavelength. It is demonstrated that the phase diffraction method becomes more effective via proper selection of the structured illumination. In the mathematical model, the scalar near field Fresnel diffraction theory is exploited by using the spatial mode of the optical fiber as an illumination. The paraxial complex ray tracing method is used to describe wave propagation through the coated optical fiber by decomposing the structured illumination wavefront into a superposition of plane waves [25]. Since the particular regions of wavefront is exposed specific phase delays due to the fact that the light wave traverses to the phase object, it causes distinct deviations on the resultant diffraction pattern which is recorded at near field region by a sensor array. In this way, the thickness information about the nanoscale thin film is obtained by matching experimental and mathematical model results.

2. Mathematical model of a transparent dielectric film on the optical fiber

The proposed mathematical model mainly based on generation of structured light, paraxial complex ray tracing method and near field Huygens–Fresnel diffraction formula. Overview of the mathematical model is given in Fig. 1.

Spatial modes of the optical fiber are used as an incident wave as shown in Fig. 1(a). The spatial distribution of the field mode from the end facet of excitation fiber is calculated via Fraunhofer far field approximation [26]:

$$\varphi_i(\rho, \theta, \alpha') = \frac{ie^{-ikr}}{\lambda r}\int_0^{2\pi}\int_0^{\infty}\varphi(\rho, \alpha)e^{ik\rho\sin\theta\cos(\alpha'-\alpha)}\rho d\rho d\alpha' \qquad (1)$$

where λ is the wavelength, φ is the propagating field mode in the optical fiber and k is the wavenumber.

Once the incident field is obtained at the front plane of the film coated optical fiber as an illumination, it is divided into m sections such that each one is represented by a ray traversing the thin film (Fig. 1(b)). Then, the phase variations of rays through the phase object can be found by paraxial complex ray tracing. The field at an arbitrary point P on the x′ plane for different regions can be expressed as:

$$\begin{aligned}
&U(P) = \varphi_i(x')\exp(ikz)\exp(-i\phi_s), \quad |x'| > c\\
&U(P) = \varphi_i(x')\exp(ikz)\exp(-i[\phi_s + \phi_d]), \quad b < |x'| < c\\
&U(P) = \varphi_i(x')\exp(ikz)\exp(-i[\phi_s + \phi_d + \phi_{cl}]), \quad a < |x'| < b\\
&U(P) = \varphi_i(x')\exp(ikz)\exp(-i[\phi_s + \phi_d + \phi_{cl} + \phi_{co}]), \quad 0 < |x'| < a
\end{aligned} \qquad (2)$$

where a, b and c are the core, the cladding and the coated optical fiber radii, respectively. Furthermore, ϕ_s, ϕ_d, ϕ_{cl} and ϕ_{co} are represented as:

$$\begin{aligned}
&\phi_s = 2kn_s c,\\
&\phi_d = 2k(n_d - n_s)\sqrt{c^2 - x'^2},\\
&\phi_{cl} = 2k(n_{cl} - n_d)\sqrt{b^2 - x'^2},\\
&\phi_{co} = 2k(n_{co} - n_{cl})\sqrt{a^2 - x'^2}
\end{aligned} \qquad (3)$$

where n_s, n_d, n_{cl} and n_{co} are refractive indices of the surrounding medium, the dielectric film, the cladding and the core, respectively.

After the wavefront is obtained at the end of film coated optical fiber, the total diffracted field on the sensor array (Fig. 1(c)) at an arbitrary point P can be found by Modified Huygens Fresnel formula (MHF) [27]:

$$U'(P) = -\frac{1}{4\pi}\sum_{x'=-\infty}^{\infty}\left(ik(1 + \cos\theta) - \frac{\cos\theta}{r'}\right)\frac{\exp(ikr')}{r'}U \qquad (4)$$

where the obliquity factor $\cos\theta = \frac{x'' - x'}{z}$.

The MHF formula includes evanescent waves and high order spatial variations via the contribution of $\frac{\cos\theta}{r'}$ term in the above equation which is called as near field term. It can be seen that the near field term starts to dominate at small distances ($r' \to 0$) and small angles ($\theta \to 0$). The intensity pattern for three layer geometry is obtained by:

$$I = (U'(P))(U'(P))^* \qquad (5)$$

The normalized intensity is obtained by equalizing the total power on the sensor array to unity.

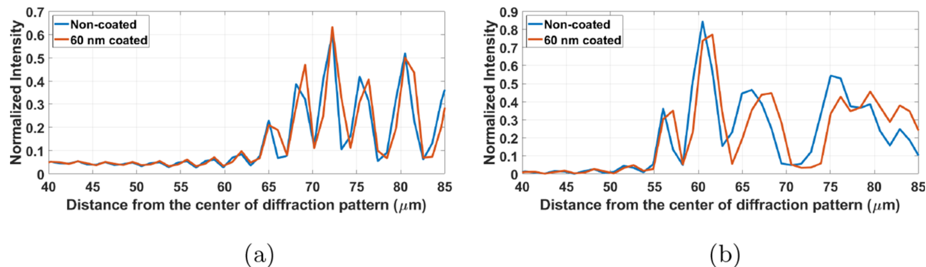

Fig. 2. Simulation results of diffraction pattern deviation between non-coated and 60 nm coated fibers at 200 μm distance with sensor array for (a) Plane wave illumination (b) LP_{11} illumination.

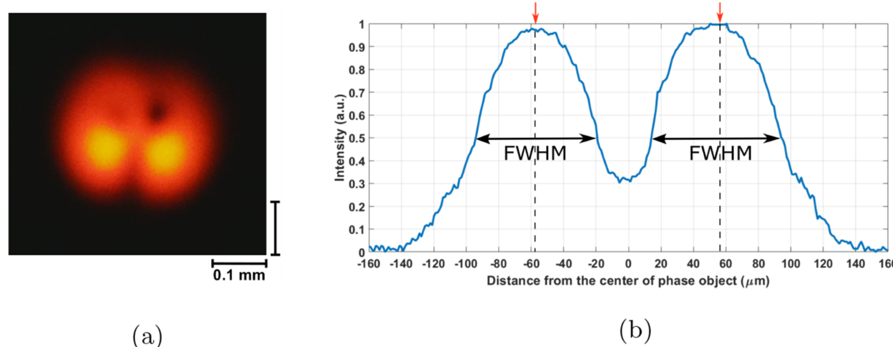

Fig. 3. Experimental LP_{11} (a) beam profile and (b) intensity distribution.

3. Experiment

In this study, we used the film coated optical fiber to represent the three layer geometry since optical fibers have perfect geometry with known optical parameters such as refractive indices and radii. The Layer by Layer Assembly (LbL) technique was chosen to build multi-layer sub-wavelength thin films because of simplicity and robustness. In this way, the thickness and roughness of the film becomes controllable on nanoscales [28]. The combination of Poly arcylic acid (PAA) and Polyethylenimine (PEI) was used to obtain transparent coating at the wavelength of interest [29]. The polymer chains penetrate to the fiber surface and show exponentially increasing film thickness.

The coating process starts with the cleaning of optical fiber with Isopropyl Alcohol. Then, the fiber was first dipped into the cationic solution (PEI) for 5 min, followed by rinsing distilled water for 30 s and drying. This process creates the first positively charged layer on the fiber. The same cycle was applied for first negatively charged layer by using PAA. The creation of first bilayer, positively and negatively charged layers, is called one deposition. Starting from the second deposition cycle, the dipping times reduced to 3 min. This process is repeated to obtain desired film thickness.

The first step of the experimental testing procedure is the generation of linearly polarized mode 11 (LP_{11}) since using modal illumination source having narrower PSF has reshaped the diffraction pattern. According to the numerical simulations, although the diffraction pattern is recorded at near field region to include the effect of near field terms, the discrepancy between non-coated and coated fibers is not distinguishable in the plane wave illumination for sub-wavelength thin film thickness (Fig. 2(a)). However, when the illumination source is replaced by the structured light, the diffracted wave peak shifts and amplitude diversions between patterns become apparent (Fig. 2(b)).

We obtained the LP_{11} mode by focusing of 632.8 nm He-Ne laser beam to tip of the optical fiber such that slightly off centered. The distance between optical fibers are critical to obtain narrower PSF at regions that rays have longest optical path length in the dielectric film since they carry further information about the thickness of film. In our experiment, the distance between excitation fiber end and coated fiber is 1.3 mm. The generated mode is given in Fig. 3. It is not completely pure LP_{11} but contains a fraction of the fundamental mode (LP_{01}) as well. The full width half maximum (FWHM) of one lobe is approximately 73 μm and peak locations are at around 60 μm. To discuss the narrowness of structured illumination, we also calculated the FWHM of Gaussian beam of He-Ne laser at 1.3 mm. The result shows that it has 900 μm FWHM which is approximately twelve times greater than structured illumination FWHM.

The generated LP_{11} mode were sent to the polymer coated optical fiber. The near field diffraction pattern of the phase object was obtained via processing the image recorded by the sensor array. The sensor array has 1.12 μm pixel size and the distance between coated fiber and sensor array is 200 μm. The radius of core and cladding are $a = 4.15$ μm and $b = 62.5$ μm and the refractive indices are $n_{co} = 1.4623$ and $n_{cl} = 1.4570$, respectively. The top view of experimental setup is given in Fig. 4.

4. Results and discussion

Here we focus mainly on the film thickness close to one tenth of source wavelength. Four different samples were chosen among the tens of films for testing the procedure considering uniformity and roughness of the films. The thickness of films were estimated by matching the experimental diffraction patterns with the mathematical model results. The phase contribution due to the nanoscale thin film modify the higher

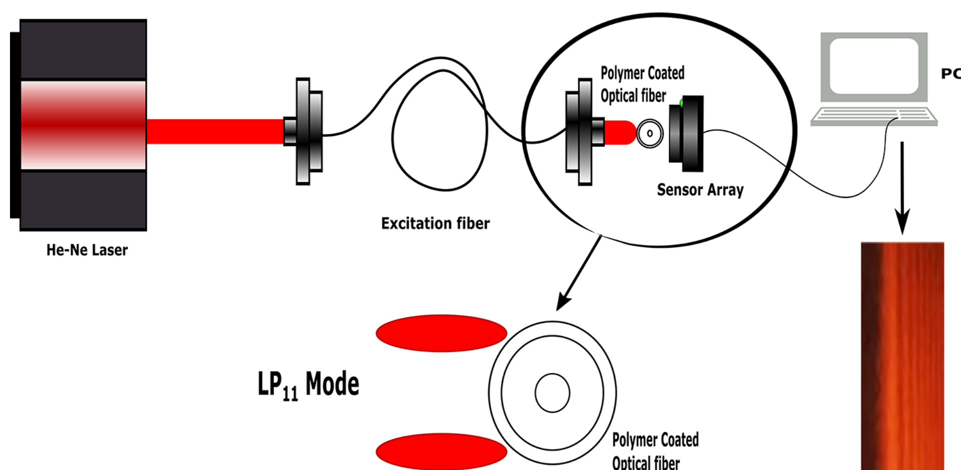

Fig. 4. Experimental setup and recorded diffraction pattern.

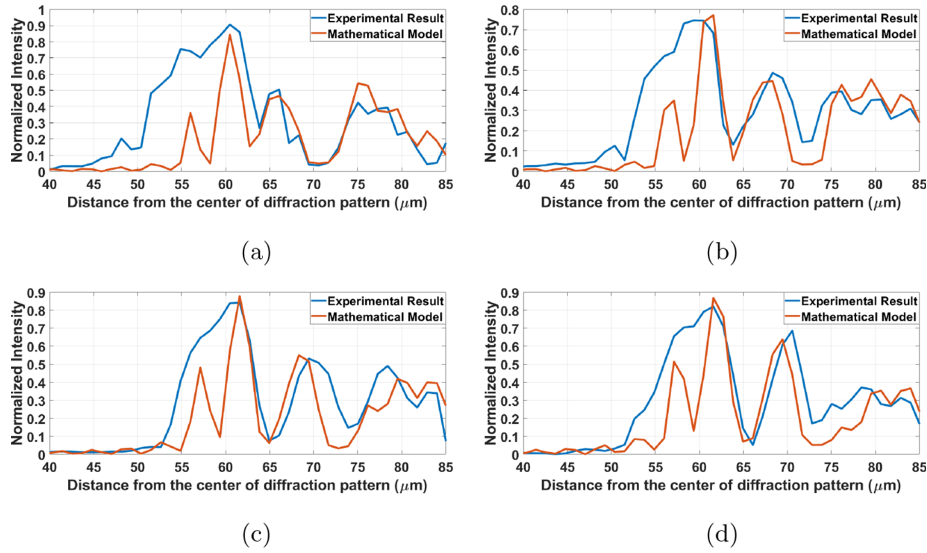

Fig. 5. Diffraction patterns of experimental (blue) and simulation (orange) results for: (a) non-coated fiber (b) 60 nm polymer coated fiber (c) 149 nm polymer coated fiber (d) 188 nm polymer coated fiber. (For interpretation of the references to colour in this figure legend, the reader is referred to the web version of this article.)

order diffraction pattern both in amplitude and width, as expected. Diffraction patterns corresponding to samples are depicted in Fig. 5.

We employ RMSLE (Root Mean Square Logarithmic Error) and differential shifts for zeroth, first and second order peaks on the diffraction pattern as metrics to assess the accurate thickness values which are given in Fig. 6. The RMSLE is the measure of relative deviations

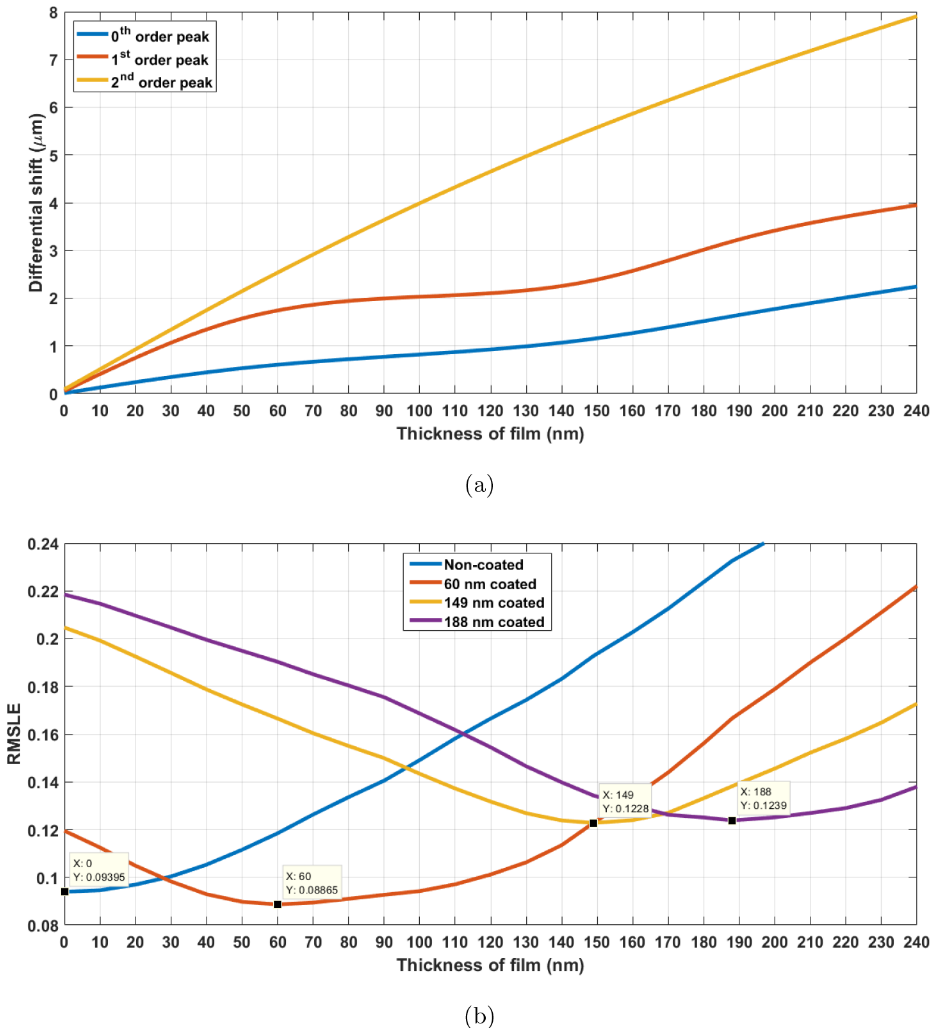

Fig. 6. (a) Zero, first and second order differential peak shifts with respect to thickness of coating (b) RMSLE for different coating thickness values.

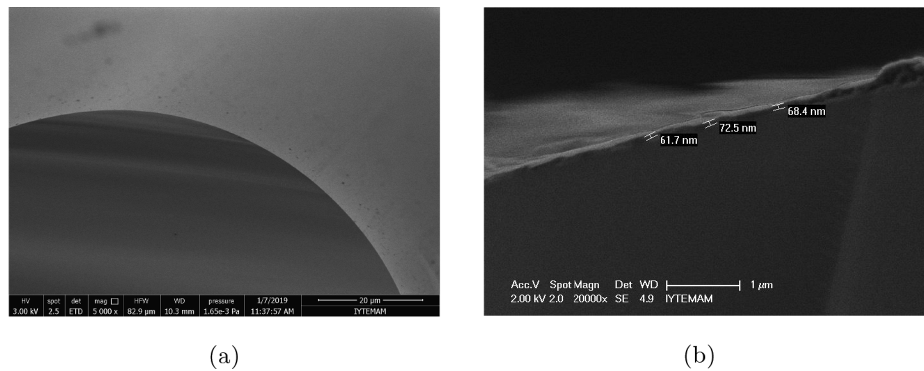

(a) (b)

Fig. 7. SEM images: (a) Non-coated optical fiber (b) 65 nm polymer coated optical fiber.

Table 1
SEM and NPD method film thickness values.

Method	Fiber-1	Fiber-2	Fiber-3	Fiber-4
SEM (nm)	$\mu_1 = 0$	$\mu_2 = 65$	$\mu_3 = 130$	$\mu_4 = 185$
	$\sigma_1 = 0$	$\sigma_2 = 28$	$\sigma_3 = 156$	$\sigma_4 = 317$
NPD (nm)	$\mu_1 = 0$	$\mu_2 = 60$	$\mu_3 = 149$	$\mu_3 = 188$

between mathematical model and experimental results. The RMSLE is calculated as:

$$\mathrm{RMSLE} = \sqrt{\frac{\sum_{i=1}^{N} (\log(I_i^{exp} + 1) - \log(I_i^{model} + 1))^2}{N}} \tag{6}$$

where I_i^{exp} and I_i^{model} are intensity values for experiment and mathematical model, respectively.

SEM images were used for the verification of the procedure. Aforementioned optical fibers were broken and examine manually to obtain surface topography of films at various cross sections as given in Fig. 7.

SEM and proposed near field phase diffraction (NPD) method results are summarized in Table 1. The table includes mean (μ) and variance (σ) values of film thickness. Since SEM uses pointwise scanning method, the average film thickness was calculated by taking measurements from different points of samples.

5. Conclusion

In this work, we have demonstrated that the near field phase diffraction method using spatially structured illumination is a powerful technique to estimate the thickness of nanoscale transparent dielectric films coated on optical fibers. It has been verified that the classical diffraction limit can be circumvented by modulating the whole PSF of system via proper selection of illumination and using the near field diffraction technique. The experimental results show that the deviation between resultant diffraction patterns for different coating thickness becomes distinguishable and measurable up to 60 nm (~$\lambda_0/10$) that is critical threshold for many sensor applications. In contrast to conventional techniques, the proposed method offers an opportunity to implement a real time automated system for quality control in optical sensor technologies. For the future works, higher order modes having narrower PSF or quantum dots can be used as an excitation source or NA of system can be further increased to obtain better resolution.

Declaration of Competing Interest

The authors declare that they have no known competing financial interests or personal relationships that could have appeared to influence the work reported in this paper.

References

[1] S.K. Mishra, B.D. Gupta, Surface plasmon resonance-based fiber-optic hydrogen gas sensor utilizing indium-tin oxide (ito) thin films, Plasmonics 7 (2012) 627–632, https://doi.org/10.1007/s11468-012-9351-7.
[2] L. Alwis, K. Bremer, T. Sun, K.T. Grattan, Analysis of the characteristics of pva-coated lpg-based sensors to coating thickness and changes in the external refractive index, IEEE Sens. J. 13 (3) (2013) 1117–1124, https://doi.org/10.1109/JSEN.2012.2230534.
[3] A.G. Leal-Junior, A. Theodosiou, C. Marques, M.J. Pontes, K. Kalli, A. Frizera, Compensation method for temperature cross-sensitivity in transverse force applications with fbg sensors in pofs, J. Light. Technol. 36 (17) (2018) 3660–3665, https://doi.org/10.1109/JLT.2018.2848704.
[4] C.A.F. Marques, A. Pospori, G. Demirci, O. Çetinkaya, B. Gawdzik, P. Antunes, O. Bang, P. Mergo, P. André, D.J. Webb, Fast bragg grating inscription in pmma polymer optical fibres: Impact of thermal pre-treatment of preforms, Sensors 17 (4) (2017) 891, https://doi.org/10.3390/s17040891.
[5] C.A.F. Marques, R. Min, A.L. Junior, P. Antunes, A. Fasano, G. Woyessa, K. Nielsen, H.K. Rasmussen, B. Ortega, O. Bang, Fast and stable gratings inscription in pofs made of different materials with pulsed 248 nm krf laser, Opt. Express 26 (2) (2018) 2013–2022, https://doi.org/10.1364/OE.26.002013.
[6] M.F. Domingues, C.A. Rodriguez, J. Martins, C. Tavares, C. Marques, N. Alberto, P. André, P. Antunes, Cost-effective optical fiber pressure sensor based on intrinsic fabry-perot interferometric micro-cavities, Opt. Fiber Technol. 42 (2018) 56–62, https://doi.org/10.1016/j.yofte.2018.02.016.
[7] A. Leal-Junior, A. Theodosiou, C. Díaz, C. Marques, M. Pontes, K. Kalli, A. Frizera-Neto, Polymer optical fiber bragg gratings in cytop fibers for angle measurement with dynamic compensation, Polymers 10 (6) (2018) 674, https://doi.org/10.3390/polym10060674.
[8] C.A.R. Díaz, C. Leitão, C.A. Marques, M.F. Domingues, N. Alberto, M.J. Pontes, A. Frizera, M.R.N. Ribeiro, P.S.B. André, P.F.C. Antunes, Low-cost interrogation technique for dynamic measurements with fbg-based devices, Sensors 17 (10) (2017) 2414, https://doi.org/10.3390/s17102414.
[9] A. Leal-Junior, A. Theodosiou, A. Frizera-Neto, M.J. Pontes, E. Shafir, O. Palchik, N. Tal, S. Zilberman, G. Berkovic, P. Antunes, P. André, K. Kalli, C. Marques, Characterization of a new polymer optical fiber with enhanced sensing capabilities using a bragg grating, Opt. Lett. 43 (19) (2018) 4799–4802, https://doi.org/10.1364/OL.43.004799.
[10] A.G. Leal-Junior, C. Marques, A. Frizera, M.J. Pontes, Dynamic mechanical analysis on a polymethyl methacrylate (pmma) polymer optical fiber, IEEE Sens. J. 18 (6) (2018) 2353–2361, https://doi.org/10.1109/JSEN.2018.2797086.
[11] G. Woyessa, K. Nielsen, A. Stefani, C. Markos, O. Bang, Temperature insensitive hysteresis free highly sensitive polymer optical fiber bragg grating humidity sensor, Opt. Express 24 (2) (2016) 1206–1213, https://doi.org/10.1364/OE.24.001206.
[12] U. Sampath, D. Kim, H. Kim, M. Song, Polymer-coated fbg sensor for simultaneous temperature and strain monitoring in composite materials under cryogenic conditions, Appl. Opt. 57 (3) (2018) 492–497, https://doi.org/10.1364/AO.57.000492.
[13] V. Mishra, M. Lohar, A. Amphawan, Improvement in temperature sensitivity of fbg by coating of different materials, Optik 127 (2) (2016) 825–828, https://doi.org/10.1016/j.ijleo.2015.10.014.
[14] M. Yang, J. Dai, Review on optical fiber sensors with sensitive thin films, Photonic Sens. 2 (1) (2012) 14–28, https://doi.org/10.1007/s13320-011-0047-y.
[15] J. Yang, X. Dong, K. Ni, C.C. Chan, P.P. Shun, Intensity-modulated relative humidity sensing with polyvinyl alcohol coating and optical fiber gratings, Appl. Opt. 54 (10) (2015) 2620–2624, https://doi.org/10.1364/AO.54.002620.
[16] B. Maniscalco, P.M. Kaminski, J.M. Walls, Thin film thickness measurements using scanning white light interferometry, Thin Solid Films 550 (2014) 10–16, https://doi.org/10.1016/j.tsf.2013.10.005.
[17] H. Yoshino, A. Abbas, P.M. Kaminski, R. Smith, J.M. Walls, D. Mansfield, Measurement of thin film interfacial surface roughness by coherence scanning interferometry, J. Appl. Phys. 121 (10) (2017) 105303, , https://doi.org/10.1063/1.4978066.
[18] J.N. Hilfiker, M. Stadermann, J. Sun, T. Tiwald, J.S. Hale, P.E. Miller, C. Aracne-Ruddle, Determining thickness and refractive index from free-standing ultra-thin

polymer films with spectroscopic ellipsometry, Appl. Surf. Sci. 421 (2017) 508–512, https://doi.org/10.1016/j.apsusc.2016.08.131.

[19] C.J. Tang, R.S. Chang, C.Y. Han, Using imaging ellipsometry to determine angular distribution of ellipsometric parameters without scanning mechanism, Opt. Lasers Eng. 77 (2016) 39–43, https://doi.org/10.1016/j.optlaseng.2015.07.010.

[20] J.W. Goodman, Introduction to Fourier Optics, Roberts and Company Publishers, 2005.

[21] I. Izeddin, M. El Beheiry, J. Andilla, D. Ciepielewski, X. Darzacq, M. Dahan, Psf shaping using adaptive optics for three-dimensional single-molecule super-resolution imaging and tracking, Opt. Express 20 (5) (2012) 4957–4967, https://doi.org/10.1364/OE.20.004957.

[22] M. Paúr, B. Stoklasa, Z. Hradil, L.L. Sánchez-Soto, J. Rehacek, Achieving the ultimate optical resolution, Optica 3 (10) (2016) 1144–1147, https://doi.org/10.1364/OPTICA.3.001144.

[23] Ç. Ekici, M.S. Dinleyici, A practical approach for optical characterization of a film coated on the optical fiber, Opt. Fiber Technol. 36 (2017) 382–386, https://doi.org/10.1016/j.yofte.2017.05.015.

[24] L. Novotny, B. Hecht, Principles of Nano-optics, 2nd ed., Cambridge University Press, 2012.

[25] F.A. Volpe, P.D. Létourneau, A. Zhao, Huygens-fresnel wavefront tracing, Comput. Phys. Commun. 212 (2017) 123–131, https://doi.org/10.1016/j.cpc.2016.10.021.

[26] R.K. Boncek, D.L. Rode, Far field radiation and modal dispersion of 1310 nm dispersion-optimized fiber at 850 nm, J. Light. Technol. 9 (1) (1991) 18–21, https://doi.org/10.1109/50.64918.

[27] K.G. Makris, D. Psaltis, Huygens-fresnel diffraction and evanescent waves, Opt. Commun. 284 (6) (2011) 1686–1689, https://doi.org/10.1016/j.optcom.2010.10.001.

[28] Y.H. Yang, M. Haile, Y.T. Park, F.A. Malek, J.C. Grunlan, Super gas barrier of all-polymer multilayer thin films, Macromolecules 44 (6) (2011) 1450–1459, https://doi.org/10.1021/ma1026127.

[29] L. Zhang, H. Liu, E. Zhao, L. Qiu, J. Sun, J. Shen, Drying and nondrying layer-by-layer assembly for the fabrication of sodium silicate/TiO2 nanoparticle composite films, Langmuir 28 (3) (2012) 1816–1823, https://doi.org/10.1021/la2043125.